Electromagnetic Modeling of Passive Circuit Elements in MMIC

David C. Chang, *Fellow, IEEE,* and Jian X. Zheng, *Student Member, IEEE*

***Abstract*—A spatial-domain mixed-potential integral equation method is developed for the analysis of microstrip discontinuities and antennas of arbitrary shape. The algorithm is based on roof-top basis functions on a rectangular and triangular mixed grid and analytical evaluation of the quadruple moment integrals involved. The algorithm is successfully implemented into an accurate, efficient and versatile computer program. The numerical results agree with the measured ones very well.**

I. Introduction

IT IS COMMONLY accepted that electromagnetic modeling and CAD are much needed to achieve a first-pass design for monolithic microwave/millimeter-wave integrated circuits (MMIC). As the operating frequency and functionality of these chips continue to increase, our inability to accurately model the effect of junction discontinuities and parasitic coupling among circuit elements is quickly becoming a critical bottleneck in ensuing a successful design. For operating frequencies beyond 20 GHz for a typical circuit, traditional quasi-static [1], [2] and other waveguide methods [3], [4] can no longer be expected to yield accurate results. In this paper, we shall present the algorithmic development of a full-wave method and its application to microstrip structures of general shape. We believe that this method is not only computationally efficient, but also yields a physical interpretation compatible to the physical picture as to how the current waves should behave on a microstrip, particularly near a junction region.

The algorithm we developed, called P(seudo)-mesh, is derived from the application of moment method to a mixed-potential integral equation (MPIE) in spatial domain for finding both current and charge distributions on the microstrip surface. The formulation of the integral equation itself can be traced back to the well-known work of Harrington [5]. For planar structures, it has at least two distinctive advantages when compared with a typical electric field integral equation (EFIE): one is that the Green's functions involved in the kernel of a MPIE are scalar functions of electric and magnetic types and they can be represented typically by one-dimensional Sommerfeld integrals. The other is that the singularity in the Green's functions of both types is of the order of $1/R$, where $R = |\bar{r} - \bar{r}'|$ is the distance between the source and observation points; the moment integrals associated with this singular term are, in fact, known analytically in closed-form. For a planar structure s as shown in Fig. 1, the MPIE can be written down as

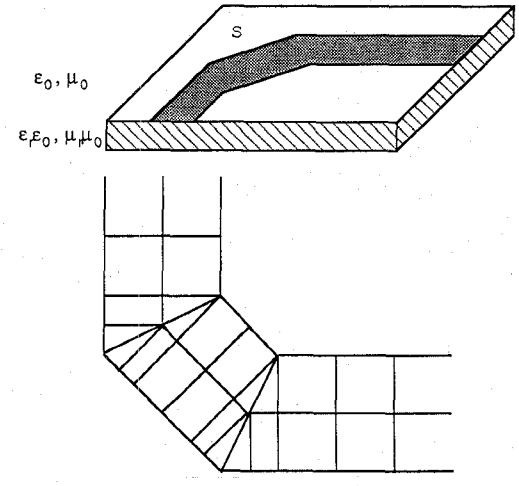

Fig. 1. A microstrip circuit and its gridded structure.

$$\frac{j\omega\mu_0}{4\pi}\int_s ds\int_s ds'\left[G_m(\bar{r},\bar{r}')\bar{T}(\bar{r})\cdot\bar{J}(\bar{r}') - \frac{1}{k_0^2}G_e(\bar{r},\bar{r}')\,\nabla\cdot\bar{T}(\bar{r})\,\nabla'\cdot\bar{J}(\bar{r}')\right] = \int_s ds\bar{E}_i(\bar{r})\cdot\bar{T}(\bar{r}) \quad (1)$$

where G_e and G_m are the Green's functions of electric and magnetic types; $\bar{J}(\bar{r}')$ and $\bar{T}(\bar{r})$ are, respectively, the current distribution and the test function, which satisfy the boundary condition on the structure; k_0 and μ_0 are, respectively, the wavenumber and permeability in free space, ω is the angular frequency; and $\bar{E}_i$ is the impressed electric field on the structure. When the source point (x', y', z') and the field point (x, y, z) are on the same plane,

Manuscript received August 7, 1990; revised January 14, 1992. This work was supported by the Center for Microwave/Millimeter-Wave Computer-Aided Design, University of Colorado at Boulder, Boulder, CO 80309.

The authors are with the MIMICAD Center, Department of Electrical and Computer Engineering, University of Colorado at Boulder, Boulder, CO 80309-0425.

IEEE Log Number 9201710.

the Green's functions for microstrip structures are [6]

$$G_m(\rho) = \int_0^\infty 2J_0(\lambda\rho)\frac{\mu_r\lambda}{\mu_r u_0 + u_n \coth(u_n h)}\,d\lambda \tag{2}$$

$$G_e(\rho) = \int_0^\infty 2J_0(\lambda\rho)\frac{\lambda[u_0 + \mu_r u_r \tanh(u_n h)]}{[\epsilon_r u_0 + u_n \tanh(u_0 h)][\mu_r u_0 + u_n \coth(u_n h)]}\,d\lambda \tag{3}$$

where h is the thickness of the substrate; $\epsilon_0\epsilon_r$ and $\mu_0\mu_r$ are the dielectric permittivity and permeability, respectively; $J_0(\lambda\rho)$ is the zero-th order Bessel function.

$$\rho = \sqrt{(x - x')^2 + (y - y')^2} \tag{4}$$

$$u_0 = \sqrt{\lambda^2 - 1}; \qquad \mathrm{Re}\,(u_0) \geq 0,\ \mathrm{Im}\,(u_0) \geq 0 \tag{5}$$

$$u_n = \sqrt{\lambda^2 - \epsilon_r\mu_r}; \qquad \mathrm{Re}\,(u_n) \geq 0,\ \mathrm{Im}\,(u_n) \geq 0. \tag{6}$$

The MPIE formulation has been previously adopted by several authors to model microstrip structures, both in the form of microstrip patch antennas and microstrip circuit discontinuities [7]–[8]. For instance, in the works by Wu, et al. [7], a microstrip structure is divided into two sets of rectangular cells and pulse basis functions are used to approximate the charge and current distribution separately. Special form of linear "roof-top" basis functions is used to approximate the current distribution by Mosig in [8], again for a set of rectangular cells. These methods obviously are most appropriate when the structure under investigation can be, in fact, naturally divided into rectangular cells, but would not be as efficient when cells of reasonable size (about 20 cells per waveguide wavelength) cannot be fitted into the boundaries of a structure. On the other hand, a full implementation of roof-top basis functions for triangular cells has been reported recently [15]. The current distribution in a given cell is expressed in terms of the nodal currents at its vertices. Boundary conditions at the edge of a microstrip structure are difficult to enforce in this case, particularly when non-rectangular corners are encountered. Furthermore, it has been demonstrated in [15] that, for a given structure, the rate of convergence for such a scheme may depend upon the particular orientation of the cells selected.

The new algorithm presented here uses a combination of rectangular and triangular cells in a self-consistent manner in order to take into account the regularity in shape over the major portion of a microstrip structure, while still preserving the flexibility to model junctions of arbitrary shape locally. It embodies the advantages of the methods described above but without their respective disadvantages. As it will become clear later, it also has a very attractive physical interpretation, which in turn lends itself naturally to the choice of cells for a given geometry. Mixed use of rectangular cells and triangular cells and the derivation can be found in finite element analysis in the solution of scalar integral or differential equations [16]. Special consideration has to be taken for our solution of vector current distribution, whose normal component, instead of itself, is continuous on cell boundaries, on a microstrip structure.

II. Roof-Top Basis Functions

As stated in the introduction, what distinguishes the P-mesh from other similar use of roof-top basis functions to approximate the current distribution on a microstrip structure is that we are able to mix rectangular cells and triangular cells in a self-consistent manner as shown in Fig. 1. This self-consistency is derived from the observation that in order to avoid the unphysical occurence of a δ-function charge density in the numerical process, only the normal component of the current density, but *not* the current density itself, is required to be continuous across a cell boundary. Thus, instead of expressing the current distribution in terms of *vector* nodal currents at the three vertices of a triangular cell [15], we can implement a modified version in which the current distribution is expressed in terms of the normal components on the three sides [17]. In order to solve for the current uniquely, we further impose an additional requirement that these normal components have to remain constant across their respective boundaries. In the case of a rectangular cell, two of the four additional conditions can be shown as redundant and thus the number of equations is again reduced to six for the six unknown coefficients.

2.1 Roof-Top Functions on Rectangular Cells

Denote the side formed by nodes i and j as side (i, j). We can express the current density distribution $\bar{J}_\alpha(x, y)$ in rectangle α in terms of the normal component $I_\alpha^{i,j}$ on the sides, where the subscript α and the superscripts i, j mean the side (i, j) of cell α:

$$\bar{J}_\alpha(x, y) = \sum_{i=1}^{4} I_\alpha^{i,i+1}\bar{D}_\alpha^{i,i+1}(x, y) \tag{7}$$

where $\bar{D}_\alpha^{i,i+1}$ is the expression for the corresponding roof-top function to the side $(i, i + 1)$ of cell α (see Fig. 2). Since a rectangular cell has four vertices or nodes, we can consider i as a cyclic number so that $i = i - 4$ for $i > 4$ and $i = i + 4$ for $i < 1$. It is not difficult to show that $\bar{D}_\alpha^{i,i+1}$, which has a magnitude of 1 on side $(i, i + 1)$ and vanishes on the opposite side, i.e. side $(i + 2, i + 3)$ as shown in Fig. 2, is given by

$$\bar{D}_\alpha^{i,i+1}(x, y) = \frac{[(y_{i+1} - y_i)(x - x_{i-1}) - (x_{i+1} - x_i)(y - y_{i-1})]}{\Delta_{i-1,i,i+1}} \cdot \frac{(x_{i-1} - x_i)\hat{x} + (y_{i-1} - y_i)\hat{y}}{d_{i-1,i}};$$
$$(x, y) \in \text{rectangle } \alpha \tag{8}$$

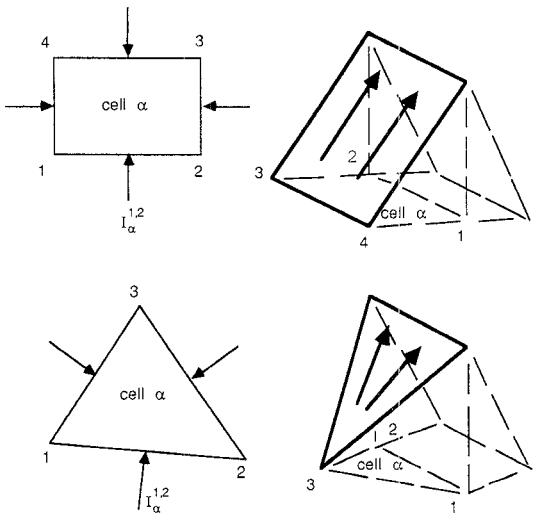

Fig. 2. The roof-top functions on a rectangular cell and a triangular cell.

$$d_{i,j} = \sqrt{(x_i - x_j)^2 + (y_i - y_j)^2} \tag{9}$$

$$\Delta_{i-1,i,i+1} = \begin{vmatrix} 1 & x_{i-1} & y^{i-1} \\ 1 & x_i & y_i \\ 1 & x_{i+1} & y_{i+1} \end{vmatrix} \tag{10}$$

and $\hat{x}$, $\hat{y}$ are the unit vectors, respectively, in the x and y-directions. The divergence of the cell current density distribution can be written as

$$\nabla \cdot \bar{J}_\alpha(x, y) = \sum_{i=1}^{4} I_\alpha^{i,i+1} Q_\alpha^i; \qquad (x, y) \in \text{rectangle } \alpha \tag{11}$$

where

$$Q_\alpha^i = -\frac{1}{d_{i-1,i}} \tag{12}$$

2.2 Roof-Top Functions on Triangular Cells

Like in the case of a rectangular cell, the current density on a triangular cell α is given by

$$\bar{J}_\alpha(x, y) = \sum_{i=1}^{3} I_\alpha^{i,i+1} \bar{D}_\alpha^{i,i+1}(x, y); \qquad (x, y) \in \text{triangle } \alpha \tag{13}$$

$$\nabla \cdot \bar{J}_\alpha(x, y) = \sum_{i=1}^{3} I_\alpha^{i,i+1} Q_\alpha^i; \qquad (x, y) \in \text{triangle } \alpha \tag{14}$$

where the roof-top functions $\bar{D}_\alpha^{i,i+1}$ are now

$$\bar{D}_\alpha^{i,i+1}(x, y) = -\frac{d_{i,i+1}}{|\Delta_{i-1,i,i+1}|} \cdot [(x - x_{i-1})\hat{x} + (y - y_{i-1})\hat{y}] \tag{15}$$

$$Q_\alpha^i = -\frac{2d_{i,i+1}}{|\Delta_{i-1,i,i+1}|} \tag{16}$$

and $i = i - 3$ for $i > 3$, or $i = i + 3$ for $i < 1$.

Unlike that for a rectangle, the roof-top basis function for a triangle changes direction at different locations. For triangle α as shown in Fig. 2, the roof-top function for side $(i, i + 1)$ is a vector parallel to side $(i - 1, i)$ at node i, parallel to side $(i - 1, i + 1)$ at node $(i + 1)$ and vanished at node $(i - 1)$. The incoming normal component is defined as 1 on side $(i, i + 1)$.

2.3 Pseudo-Mesh Current Distribution Representation

Since for both rectangular and triangular cells we can now express the current by the normal current density across the cell boundary and since each of these normal current densities is assumed to be constant along the boundary, we can now characterize the current in the cell by the *total current flow* into and out of each cell. Topologically, this is the same as replacing a microstrip structure by equivalent meshes, and the current distribution on the surface area of a cell by the current flow along corresponding meshes as shown in Fig. 3. Unlike a real mesh structure, however, the net amount of total current flows into and out of a "junction" does not follow the conventional Kirchhoff's law. In fact, the difference between the incoming current and the outgoing current contributes to the charge distribution on the cell. The requirement that the normal component of current must vanish at the edges of a microstrip circuit can be easily implemented by "opening" the corresponding meshes connecting the edges. We should note that the use of triangular "meshes" fully captures the physical phenomenon of a current flow round the corner of a bend. Thus, one of the advantages for the P-mesh representation is that it can be constructed according to the physical intuition a designer has, and such intuition usually results in fast convergence of the computational process.

2.4 The Global Expression for Current Distribution

In Section II, we have discussed the roof-top basis functions on individual cells. To complete the P-mesh development, we still need to integrate the individual current unknown, i.e. $I_\alpha^{i,i+1}$ for the cell α into a global set of "mesh" current I_m, $m = 1, 2, \cdots, M$, where M is the total number of the interconnecting meshes. As we mentioned earlier, meshes at the boundary of a microstrip structure are "disconnected" since the normal current at the edge of a boundary cell is zero. For adjacent cells α and α' as shown in Fig. 4, at the common boundary describable either by $(\alpha; i, i + 1)$ or $(\alpha'; i', i' + 1)$, the unknown current across this boundary is now expressed in terms of the mesh current I_m so that

$$I_m = I_\alpha^{i,i+1} = -I_{\alpha'}^{i',i'+1}. \tag{17}$$

The roof-top basis function corresponding to this unknown current is

$$\bar{H}_m = \bar{D}_\alpha^{i,i+1} - \bar{D}_{\alpha'}^{i',i'+1}. \tag{18}$$

It should be noted that $\bar{D}_\alpha^{i,i+1}$ is defined only in cell α, while $\bar{D}_{\alpha'}^{i',i'+1}$ is defined only in cell α'. The divergence

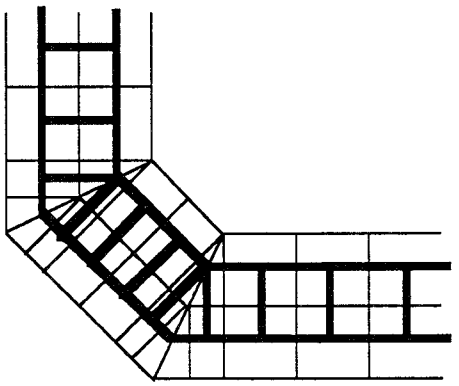

Fig. 3. The current flow in a wire mesh.

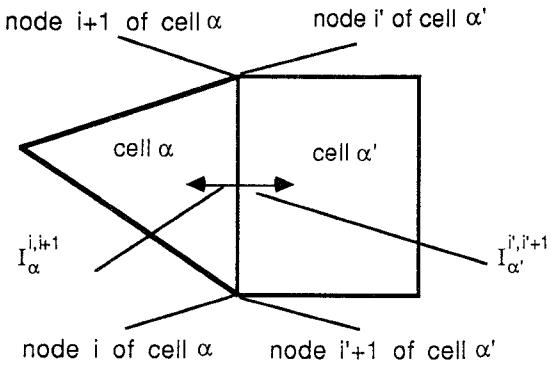

Fig. 4. The side current for two adjacent cells.

of the roof-top basis function is

$$P_m = Q_\alpha^i - Q_{\alpha'}^{i'}. \tag{19}$$

Therefore, the P-mesh current distribution on a structure can finally be expressed as

$$\bar{J}(x, y) = \sum_{m=1}^{M} I_m \bar{H}_m(x, y) \tag{20}$$

where M is the number of the unknown interconnecting "meshes."

III. Matrix Solution to the MPIE

Using each of the $\bar{H}_m(x, y)$ as the test functions in (1) and substituting (20) into (1) yield a matrix equation:

$$\sum_{m'=1}^{M} I_{m'} Z_{m,m'} = V_m; \qquad m = 1, 2, \cdots, M \tag{21}$$

where

$$Z_{m,m'} = \frac{j\omega\mu_0}{4\pi} \int_{s_m} ds \int_{s_{m'}} ds' K_{m,m'}(x, y; x', y') \tag{22}$$

$$K_{m,m'}(x, y; x', y') = G_m(\rho)\bar{H}_m(x, y) \cdot \bar{H}_{m'}(x', y') - \frac{1}{k_0^2} G_e(\rho) P_m P_{m'} \tag{23}$$

$$V_m = \int_{s_m} ds\, \bar{H}_m(x, y) \cdot \bar{E}_i(x, y) \tag{24}$$

$$\rho = \sqrt{(x - x') + (y - y')^2}. \tag{25}$$

The surface integration on s_m has to be carried out over the two adjacent cells, s_α and $s_{\alpha'}$ which share a common boundary or "mesh" m, i.e. $m = (\alpha; i, i + 1) = (\alpha'; i', i' + 1)$. The matrix element $Z_{m,m'}$ consists of quadruple integrals of the form

$$\int_{\text{cell}\,\alpha} ds \int_{\text{cell}\,\alpha'} ds' G_{m,e}(\rho) x^\mu y^\nu x'^{\mu'} y'^{\nu'};$$

$$\mu, \nu, \mu', \nu' \geq 0 \;\&\; 0 \leq \mu + \nu, \mu' + \nu' \leq 1 \tag{26}$$

For planar structures, the $G_{m,e}$ in (26) are Sommerfeld integrals (see (2) and (3)), and cannot be solved analytically. It is noticed that the Green's functions $G_{e,m}$ are only one-dimensional functions of ρ. We can evaluate them numerically first and then curve-fit them into polynomials over the range of ρ determined by the maximum and minimum distance between two cells α and α' [19]:

$$G_{m,e}(\rho) = \sum_{p=-1}^{N_p} C_p^{m,e} \rho^p \tag{27}$$

where $C_p^{m,e}$ are the coefficients from curve-fitting, N_p is the order of the polynomials. With these semi-analytical expressions of the Green's functions, the integrals in (26) are simplified as

$$Q(\alpha, \alpha', \mu, \nu, \mu', \nu', p) = \int_{\text{cell}\,\alpha} ds \int_{\text{cell}\,\alpha'} ds' \rho^p x^\mu y^\nu x'^{\mu'} y'^{\nu'};$$

$$p = -1, 0, \cdots, N_p. \tag{28}$$

Analytical solutions to the integrals with even p in (28) can be found in many books on finite elements [20]. But no formulation has been found to deal with the integrals with odd p. The integrals with odd p are solved analytically in [19]. The derivation is very complicated and it will not be included in this paper.

IV. De-Embedding of Network Parameters

In practical applications, we assume a gap voltage source at the far end of a feed line as the excitation. When the feed line is long enough, the current distribution is very close to a sinusoidal function just $0.1 \sim 0.2\lambda_g$ away from junctions, a measure of current standing wave at each port leads directly to the scattering matrix of the microstrip structure [19]. Thus, unlike those methods which use the input admittance, or the current at the voltage source [13], the scattering matrix does not require the knowledge, nor the confusion arising from the definition of the characteristic impedance of a microstrip line. Several de-embedding techniques have been developed during the course of this work, and the most accurate scheme is a three-point curve-fitting scheme. The current distribution at three uniformly-spaced points is detected to provide three equations

$$z = -z_0\text{: } J_1 = a \exp(\gamma z_0) - b \exp(-\gamma z_0) \tag{29}$$

$$z = 0\text{: } J_2 = a - b \tag{30}$$

$$z = z_0\text{: } J_3 = a \exp(-\gamma z_0) - b \exp(\gamma z_0) \tag{31}$$

where a and b are the amplitudes of the incident wave and reflected wave at $z = 0$, respectively. Summation of (29) and (31) yields

$$2(a - b)\cosh(\gamma z_0) = (J_1 + J_3). \tag{32}$$

Substituting (30) into (32) gives

$$\cosh(\gamma z_0) = \frac{J_1 + J_3}{2J_2}. \tag{33}$$

Unique γ can be solved from (33) as long as $Im(\gamma)z_0 < (\pi/2)$. Then, the incident and reflected waves can be obtained from either two of (29), (30) and (31).

The advantage of the de-embedding technique over the typical VSWR method used in experimental procedure is that we don't need to care about high standing waves since we always deal with the real part and imaginary part instead of the magnitude of current. This feature makes it very convenient to solve a multi-port network problem by just changing the excitation states instead of using matched loads.

V. Numerical Results

The P-mesh algorithm has been well implemented into a versatile computer code. It has been used to analyze various kinds of microstrip circuits and antennas. Before we proceed to discuss some examples, it is necessary to define some commonly used notations:

ϵ_r	substrate dielectric constant;
h	substrate thickness;
σ	microstrip conductivity;
w	microstrip line width;
λ_g	waveguide wavelength;
$\gamma = \alpha + j\beta$	complex propagation constant of a microstrip line;
N_w	number of cells per waveguide wavelength;
N_t	number of cells in transverse direction;
N_c	number of cells in a structure.

No obvious convergence but an error bound is observed. To give an idea what the accuracy is of the P-mesh code with $N_t = 1$ and $N_w = 20$ when the microstrip width is less than $5\%\ \lambda_g$, we list the error bounds for the cases of large values and small values of the main parameters in Table I (Note: small values are approximately defined as $|S_{i,j}| < -30$ dB and $\angle S_{i,j} < 5°$, and large values are approximately defined as $|S_{i,j}| >> 0.1$ and $\angle S_{i,j} >> 5°$). In the following analysis, we always use $N_t = 1$ and $N_w = 20$.

The first example is the double-stub structure as shown in Fig. 5. It was previously fabricated and measured for the purpose of determining the parasitic coupling of two parallel stubs [21]. Two local minima are observed in the response of $|S_{2,1}|$ (see Fig. 5). It happens even the stub separation is as large as $\lambda_g/4$. Since the two stubs are identical in length, only one minimum is expected if we break the structure into two single stubs and connect them without considering the coupling effect. But, when we consider it as a four-port network first, and then terminate the two ports with open-ends, we can always get the double minima [23]. Obviously, the double minimum response is not caused by the radiation from the open-ends, but created by the mutual coupling between the two junctions and stubs. We can also see from Fig. 5 that the theoretical results agree with the measured ones very well. There is a 1.5% difference in the resonant frequency between the numerical and experimental results, but it is within the fabrication error bound (2%).

TABLE I
THE ERROR BOUNDS FOR THE MAIN PARAMETERS

Parameter	Small Value	Large Value
λ_g	<0.5%	<0.5%
Resonant frequency	<0.5%	<0.5%
$\lvert S_{i,j}\rvert$	<2.0 dB	<1.5%
$\angle S_{i,j}$	<0.2°	<1.5%

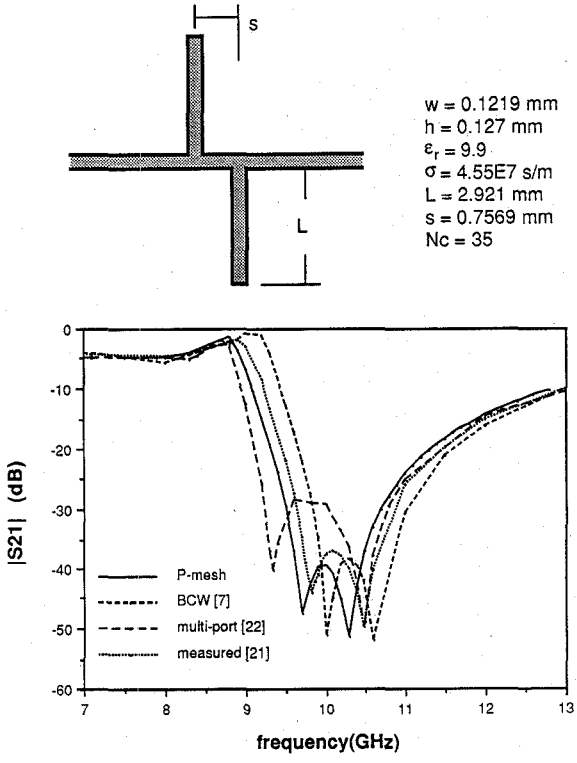

Fig. 5. A double-stub structure and its frequency response.

The other example is a serpentile line formed by three cascaded U-bends as shown in Fig. 6. Fig. 7 shows the frequency responses. It is predicted that $|S_{1,1}| < 0.2$ and $|S_{2,1}| > 0.966$ for a single U-bend, while $|S_{1,1}| < 0.05$ for a double-bend portion (see Fig. 6). Obviously, the accumulation of the reflections from the junctions has degraded the performance of the circuit. In fact, the circuit performance is also affected by the mutual coupling in the circuit. The effect of mutual coupling can easily be demonstrated by comparing the frequency responses of the three cascaded U-bends calculated in two different ways: (1) three U-bends analyzed as a whole entity (three U-bends 1); (2) three U-bends analyzed as the cascading

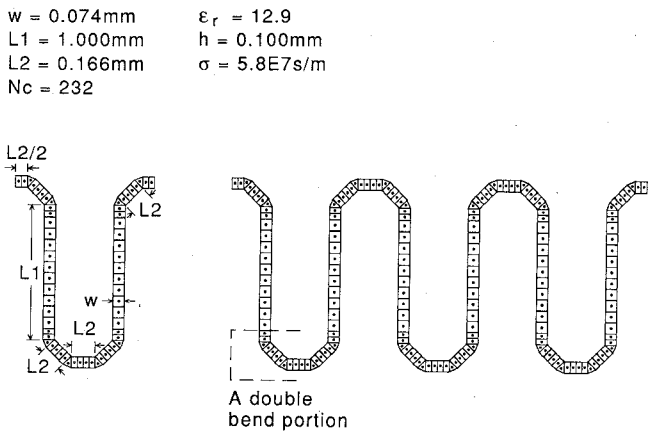

Fig. 6. A serpentile line formed by three U-bends.

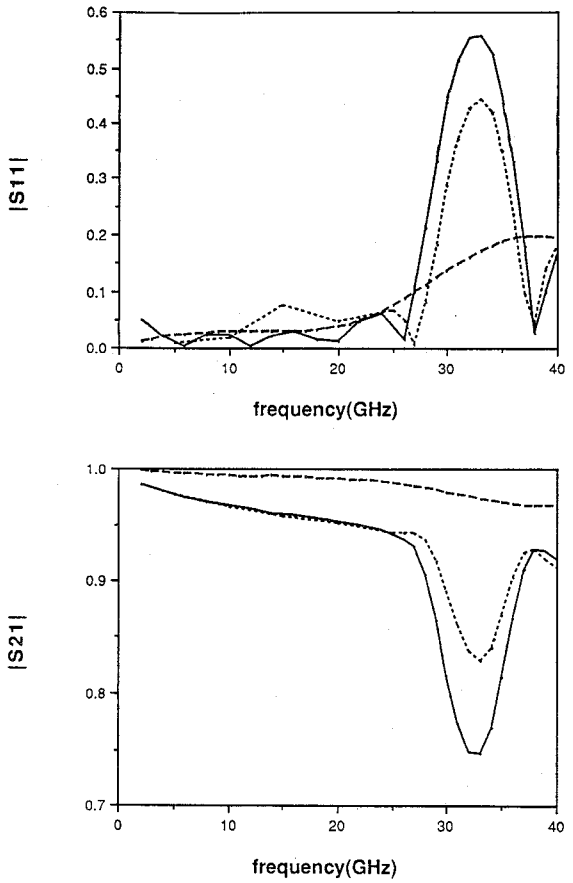

Fig. 7. The frequency responses of the U-bends.

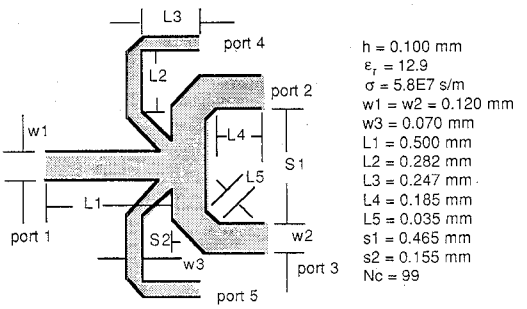

Fig. 8. A complex five-port junction.

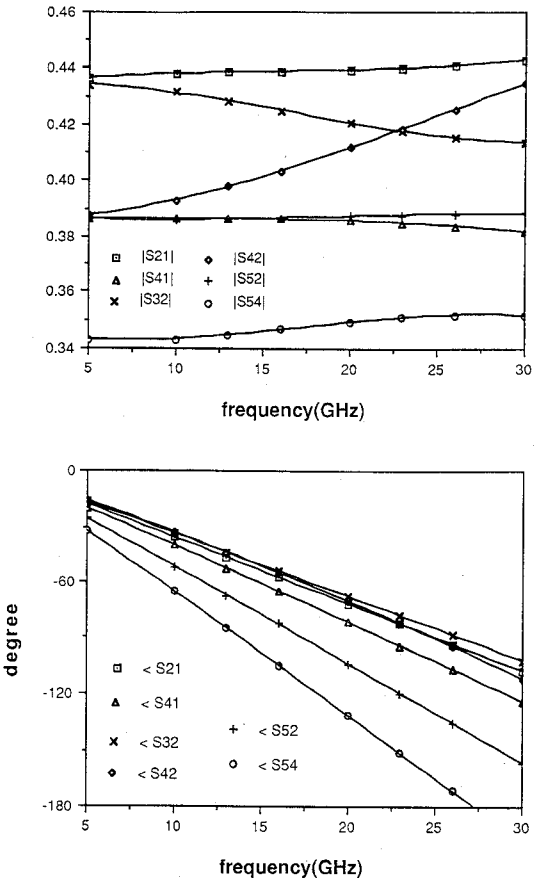

Fig. 9. The frequency responses of the five-port junction.

of three individual U-bends (three U-bends 2). A strong resonance is predicted at 32 GHz resulting from multiple reflections. It is noticed that there are substantial differences in the frequency responses of the three U-bends, especially at the resonance, between the two cases. When the coupling is included, we have $|S_{1,1}|^2 = 0.31$ and $|S_{2,1}|^2 = 0.57$. But when the coupling is omitted, $|S_{1,1}|^2 = 0.19$ and $|S_{2,1}|^2 = 0.69$ are predicted. Obviously, the differences account for the mutual coupling among the U-bends. It has been found that the radiation loss is not significant in a typical MMIC circuit [18]. The power loss in this case is $1 - |S_{1,1}|^2 - |S_{2,1}|^2 = 0.12$ and attributes to the conductor loss resulting from imperfect conductor, which is modeled as an impedance boundary condition (the value of the impedance is half of that used in [8] when the strip thickness is much larger than the skin depth).

To demonstrate the ability of the P-mesh algorithm and the code, we provide a brief analysis of a five-port junction (see Fig. 8). Static theory tells that $|S_{2,1}| = |S_{3,2}|$ and $|S_{4,1}| = |S_{4,2}| = |S_{5,2}|$. This is true at low frequency. But the high frequency responses change very much (see Fig. 9). More complicated circuits can be solved in the same way.

VI. Conclusions

We have demonstrated the P-mesh algorithm and its applications in the analysis of MMIC circuits. It can also be applied to analyze microstrip antennas [24]. In fact, al-

most any planar structures can be analyzed using the P-mesh algorithm efficiently and accurately. The following conclusions appear to be in order for MMIC circuits:

1. The P-mesh algorithm and code are versatile, efficient and accurate.
2. Coupling between elements in a MMIC circuit may strong enough to change the frequency responses very much.
3. Accumulation of small reflections from junctions and bends may result in strong resonances and the resonances may cause serious power loss in a MMIC circuit.
4. Metallic loss might be a very important loss factor, especially when resonances are established.

REFERENCES

[1] A. Farrar and A. T. Adams, "Matrix methods for microstrip three-dimensional problems," *IEEE Trans. Microwave Theory Tech.*, vol. MTT-20. pp. 497–504, Aug. 1972.

[2] P. Silvester and P. Benedek, "Microstrip discontinuity capacitance for right-angle bends, T-junctions and crossings," *IEEE Trans. Microwave Theory Tech.*, vol. MTT-21, pp. 341–346, May 1973.

[3] R. Chadha and K. C. Gupta, "Segmentation method using impedance matrices for analysis of planar microwave circuits," *IEEE Trans. Microwave Theory Tech.*, vol. MTT-29, pp. 71–74, Jan. 1981.

[4] T. S. Chu and T. Itoh, "Comparative study of mode matching formulations of microstrip discontinuity problems," *IEEE Trans. Microwave Theory Tech.*, vol. MTT-33, pp. 1018–1023, Oct. 1985.

[5] R. F. Harrington, *Field Computations by Moment Methods*. New York: Macmillan, 1968, Ch. 4.

[6] B. L. Brim and D. C. Chang, "Accelerated numerical computation of the spatial domain dyadic Green's functions of a grounded dielectric slab," *National Science Meeting Dig.*, p. 164, Boulder, CO, Jan. 1987.

[7] D. I. Wu, D. C. Chang, and B. I. Brim, "Accurate numerical modelling of microstrip junctions and discontinuities," *Int. J. Microwave Millimeter-wave Computer Aided Engineering*, to be published.

[8] J. R. Mosig, "Arbitrarily shaped microstrip structures and their analysis with a mixed potential integral equation," *IEEE Trans. Microwave Theory Tech.*, vol. 36, pp. 314–323, Feb. 1988.

[9] B. J. Rubin, "Modeling of arbitrarily shaped signal lines and discontinuities," *IEEE Trans. Microwave Theory Tech.*, vol. 37, pp. 1057–1060, June 1989.

[10] W. Wertgen and R. H. Jansen, "Efficient direct and iterative electrodynamic analysis of geometrically complex MIC and MMIC structures," *Int. J. Numerical Modelling: Electronic Networks, Devices and Fields*, vol. 2, pp. 153–186, Feb. 1989.

[11] R. W. Jackson, "Full-wave, finite element analysis of irregular microstrip discontinuities," *IEEE Trans. Microwave Theory Tech.*, vol. 37, pp. 81–89, Jan. 1989.

[12] J. C. Rautio and R. F. Harrington, "Preliminary results of a time-harmonic electromagnetic analysis of shielded microstrip circuits," in *27th Automatic RF Techniques Group Conf. Dig.*, Baltimore, June 1986, pp. 121–134.

[13] P. B. Katehi and N. G. Alexopoulos, "Frequency-dependent characteristics of microstrip discontinuities in millimeter-wave integrated circuits," *IEEE Trans. Microwave Theory Tech.*, vol. MTT-33, pp. 1029–1035, Oct. 1985.

[14] R. W. Jackson and D. M. Pozar, "Full-wave analysis of microstrip open-end and gap discontinuities," *IEEE Trans. Microwave Theory Tech.*, vol. MTT-33, pp. 1036–1042, Oct. 1985.

[15] J. X. Zheng and D. C. Chang, "Convergence of the numerical solution for a microstrip junction based upon a triangular cell expansion," in *National Science Meeting Dig.*, p. 212, Boulder, CO, Jan. 1990.

[16] L. J. Segerlind, *Applied Finite Element Analysis*. New York: Wiley, 1984, pp. 27–99.

[17] D. C. Chang and J. X. Zheng, "Numerical modeling of planar circuits with pseudo meshes," *National Science Meeting Dig.*, Boulder, CO, Jan. 1990, p. 265.

[18] J. X. Zheng and D. C. Chang, "Numerical modeling of chamfered bends and other microstrip junctions of general shape in MMICs," *IEEE MTT Int. Microwave Symp. Dig.*, Dallas, May 1990, pp. 709–712.

[19] J. X. Zheng, "Electromagnetic Modeling of Microstrip Circuit Discontinuities and Antennas of Arbitrary Shape," Ph.D. dissertation, University of Colorado at Boulder, 1990, ch. 4.

[20] T. Y. Yang, *Finite Element Structural Analysis*. Englewood Cliffs, NJ: Prentice-Hall, pp. 288–296.

[21] C. Goldsmith, Texas Instrument, private communication.

[22] A. Sabban and K. C. Gupta, "A planar-lumped model for coupled microstrip line discontinuities," *IEEE Trans. Microwave Theory Tech.* Special Issue, vol. 38, Dec. 1990.

[23] K. Larson and J. Dunn, University of Colorado at Boulder, private communication.

[24] J. X. Zheng and D. C. Chang, "Computer-aided design of electromagnetically-coupled and tuned, wide band microstrip patch antennas," in *IEEE AP-Symp. Dig.*, Dallas, May 1990, pp. 1120–1123.

David C. Chang (M'67–SM'77–F'85) was born in Hupeh, China in 1941. He received the B.Sc. in electrical engineering from National Cheng-Kung University in Taiwan in 1961, M.Sc. and Ph.D. in applied physics in 1963 and in 1967, respectively, from Harvard University.

He joined the University of Colorado at Boulder in Fall 1967. He has been a Professor of Electrical and Computer Engineering since 1975, and the Department Chair from 1981–89. In Spring 1988, he became the first Director of the Center for Microwave/Millimeter-Wave Computer-Aided Design at the University of Colorado under the auspices of the National Science Foundation. The purpose of this Center is to develop industry/university cooperative research in monolithic microwave/millimeter-wave integrated circuits and antennas. It now has thirteen industrial and government R&D sponsors, and over thirty faculty and student researchers.

Dr. Chang has been active in the IEEE Antennas and Propagation Society. His professional services with the Society include: Chair, Denver/Boulder Chapter (1969–70); Associate Editor for the Transactions (1978–80) and Guest Editor for a special issue on microstrip antennas in January, 1981; Coordinator, AP Distinguished Lecturers Program (1982–85); Member, Long-range Committee (1985–86); Chair, Ad-hoc Committee for Basic Research (1985–87) and a member of the Administrative Committee (1985–88). He is the immediate past-President of the Society.

In addition to IEEE-AP, he has also been actively involved in the IEEE Society on Microwave Theory and Techniques (MTT) and in the International Union of Radio Science (URSI). He is currently a member of the Technical Subcommittee on Microwave Field Theory for MTT, and the Vice Chairman of the United States National Committee of URSI.

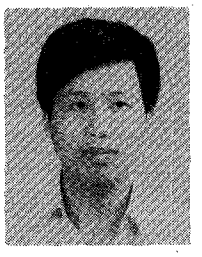

Jian-Xiong Zheng (S'91) was born in Guangdong, China in 1963. He received the B.E. degree and M.E. degree in Tsinghua University, Beijing, China in 1984 and 1986, respectively.

From 1987 to 1988, he worked in Guangdong Broadcasting Company, Guangzhou, China. During 1989 to 1990, he was a research assistant in University of Colorado at Boulder. He received the Ph.D. degree in 1990, and he is currently a research associate in University of Colorado at Boulder. His major research interests are electromagnetic theory, numerical modeling of microstrip antennas and microwave/millimeter-wave integrated circuits of general shape, and electromagnetic modeling of electronic packages.